Graphical Abstract

Spatial transcriptomics reveals unique gene expression changes in different brain regions after sleep deprivation

Yann Vanrobaeys, Zeru J. Peterson, Emily. N. Walsh, Snehajyoti Chatterjee, Li-Chun Lin, Lisa C. Lyons, Thomas Nickl-Jockschat, Ted Abel

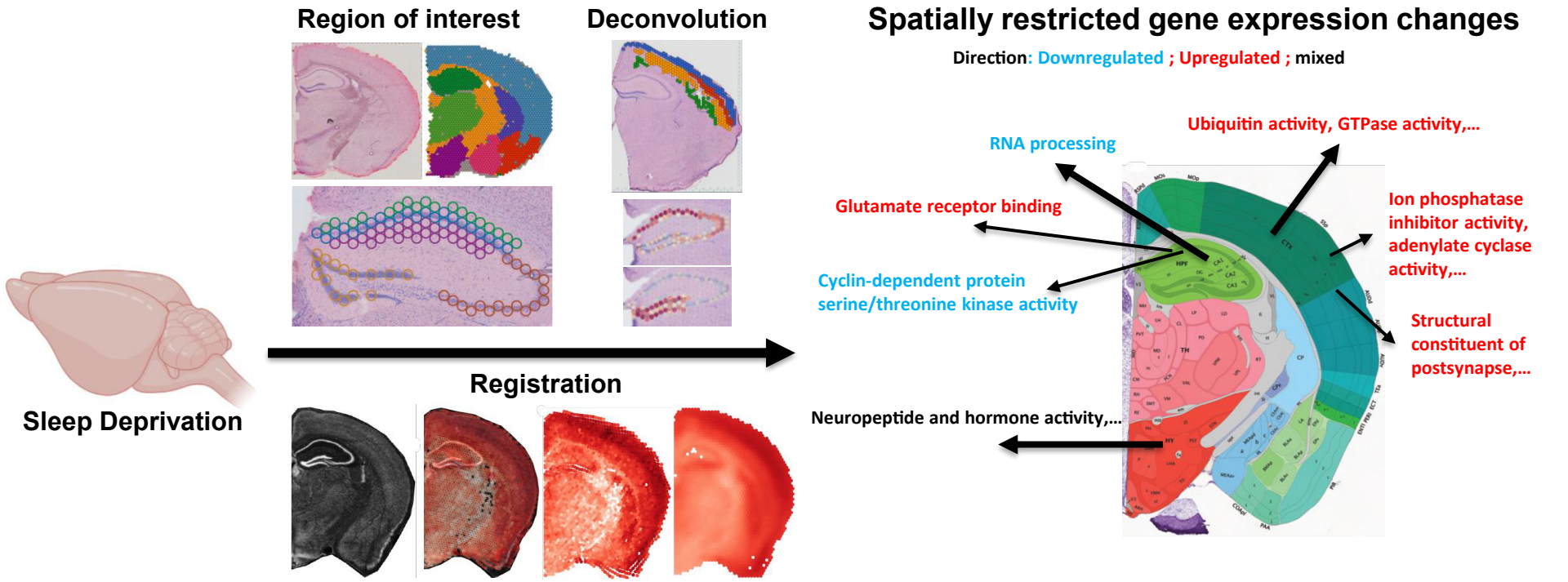

Spatial transcriptomics reveals unique gene expression changes in different brain regions after sleep deprivation

Yann Vanrobaeys[1,2,3], Zeru J. Peterson[2,5], Emily. N. Walsh[2,3,4], Snehajyoti Chatterjee[2,3], Li-Chun Lin[2,3,7], Lisa C. Lyons[6], Thomas Nickl-Jockschat[2,3,5*], Ted Abel[2,3*]

[1]Interdisciplinary Graduate Program in Genetics, University of Iowa, 357 Medical Research Center Iowa City, IA 52242, USA

[2]Iowa Neuroscience Institute, Carver College of Medicine, 169 Newton Road, 2312 Pappajohn Biomedical Discovery Building, University of Iowa, Iowa City, IA 52242, USA

[3]Department of Neuroscience and Pharmacology, Carver College of Medicine, 51 Newton Road, 2-417B Bowen Science Building, University of Iowa, Iowa City, IA 52242, USA

[4]Interdisciplinary Graduate Program in Neuroscience, University of Iowa, 356 Medical Research Center, Iowa City, IA 52242, USA

[5]Department of Psychiatry, University of Iowa, Iowa City, IA, USA

[6]Program in Neuroscience, Department of Biological Science, Florida State University, Tallahassee, FL, USA

[7]Department of Neurology, University of Iowa, Iowa City, IA, USA

* correspondence to ted-abel@uiowa.edu or thomas-nickl-jockschat@uiowa.edu

Highlights

- Spatial transcriptomics using the Visium platform reveals the transcriptional signature across the brain, recapitulating the anatomy of the mouse brain
- Sleep deprivation induces transcriptomic changes unique to each brain region
- The hippocampus is the brain region impacted the most by acute sleep deprivation, with most differentially regulated genes significantly downregulated
- The neocortex exhibits layer-specific changes in gene expression, with most differentially regulated genes significantly upregulated
- Registration of spatial transcriptomic data to a common anatomical reference space (Allen Common Coordinate Framework) allows statistical analysis of gene expression across regions of the brain and for multi-sample analysis

Abstract

Sleep deprivation has far-reaching consequences on the brain and behavior, impacting memory, attention, and metabolism. Previous research has focused on gene expression changes in individual brain regions, such as the hippocampus or cortex. Therefore, it is unclear how uniformly or heterogeneously sleep loss affects the brain. Here, we use spatial transcriptomics to define the impact of a brief period of sleep deprivation across the brain. We find that sleep deprivation induced pronounced differences in gene expression across the brain, with the greatest changes in the hippocampus, neocortex, hypothalamus, and thalamus. Both the differentially expressed genes and the direction of regulation differed markedly across regions. Importantly, we developed bioinformatic tools to register tissue sections and gene expression data into a

common anatomical space, allowing a brain-wide comparison of gene expression patterns between samples. Our results suggest that distinct molecular mechanisms acting in discrete brain regions underlie the biological effects of sleep deprivation.

Introduction

Sleep deprivation is a growing problem that effects more than one-third of adults in the U.S. and more than 70% of teenagers and adolescents[1]. Loss of sleep affects impacts cognition, attention and metabolism[2–5]. These processes are mediated by distinct neural circuits in specific brain regions—the hippocampus, the cortex, and hypothalamus, respectively. Sleep and circadian rhythm disorders have also been linked to the increased incidence and accelerated progression of neurodegenerative diseases, including Alzheimer's disease[6–10]. Given the serious consequences of sleep loss for individuals and the interaction of sleep deprivation with many diseases, it is important to understand the cellular and molecular consequences of sleep deprivation. To this end, we have used non-biased spatial transcriptomics to define whether sleep loss has distinct molecular impacts on specific brain regions.

Sleep deprivation impacts protein synthesis and gene regulation through many mechanisms including alterations to epigenetic regulation, transcription, and mRNA processing[11–19]. Estimates suggest that up to 10% of cortical transcripts are regulated with sleep/wake cycles, particularly by the length of time awake[20–22]. In the hippocampus, prolonged wakefulness causes changes in the expression of genes associated with RNA splicing, cell adhesion, dendritic localization, the synapse, and the postsynaptic membrane[11,13,23,24]. However, the brain is a highly heterogeneous organ and subserves many different functions; as brain regions and circuits differ

in their roles, they may differ dramatically in their response to sleep loss, and observations from one brain region may not be generalized to the whole brain.

New technological advances in genome-wide spatial transcriptomics offer enormous potential for providing detailed molecular maps that overcome limitations associated with single cell or single nuclear RNA sequencing (sc/snRNA-seq) and microscopy-based spatial transcriptomics methods[25]. This approach has been successfully used to generate detailed datasets and cell-type specific gene expression signatures [26–29], but it has not yet been used to profile changes in gene expression across multiple brain regions after experience. A further challenge is that a significant hurdle remains in terms of finding a strategy to align the brain regions across slices from multiple subjects or from independent experiments for data integration in multi-sample analyses. To investigate gene expression changes within the adult mouse brain after sleep deprivation, we used the 10x Genomics Visium platform, a barcoding-based, transcriptome-wide approach that generates spatial maps of gene expression. We collected gene expression data from each major brain region across a coronal brain slice, enabling us to profile multiple brain regions simulataneously. Using this technique, we were also able to get detailed, subregion and layer specific gene expression changes within the hippocampus and cortex. Finally, we present an alternative to a region-of-interest type of analysis by registering multiple slices into a common space using the Common Coordinate Framework (CCF) from the Allen Brain Atlas[30], thus adjusting for differences in the alignment of brain tissue sections and allowing for a comparison between samples. These data and analytical approaches provide a scientific resource for the neuroscientific community, and they demonstrate the diverse impact of sleep loss on gene expression across the brain.

Results

Using Visium spatial transcriptomics, we profiled spatial gene expression in coronal brain slices from sleep-deprived (SD) or control (non-sleep deprived (NSD)) adult male mice. Each coronal section covered between 1736 and 3103 spots on the Visium slides. We sequenced each sample to a median depth of 2.26E+08 (interquartile range 2.10E+08-2.37E+08), which corresponded to a mean of 93245 reads and a mean of 5978 genes per spot. We note that these rates are analogous to snRNA-seq and scRNA-seq data using the 10x Genomics Chromium platform, where a 'cell' barcode on the Chromium platform corresponds to a 'spatial' barcode on the Visium platform. However, unlike snRNA-seq data which contains high numbers of intronic reads that map to immature transcripts, we found strong enrichment of mature messenger RNAs with high mean rates of exonic alignments (mean: 88.3%; IQR: 87.7-89.4%).

We first generated region-enriched expression profiles for the samples from each condition (**Fig. 1A-C**). As expected, this approach predicted brain regions with high reliability (**Fig. 1B**) and recapitulated the brain regions from the reference coronal mouse Allen brain atlas (**Fig. 1C**). Each brain region was characterized by specific transcriptional signatures and unsupervised clustering of these region expression profiles revealed distinct clusters (**Fig. 1D**) and top biomarkers (**Fig. 1E)**. Together, these results highlight the ability of the Visium platform to achieve high-resolution spatial expression profiling across the mouse brain.

Sleep deprivation exerts differential effects on transcriptional activity in each brain region

Sleep deprivation affects different brain functions ranging from cognition and affective processing that each rely upon distinct neuronal circuits[17,22–24,31–34]. However, little is known

about how sleep deprivation alters transcriptomic activity in individual brain regions, as bulk sequencing approaches inevitably average out regionalized effects. To address this problem, we performed differential gene expression analysis in each of the brain regions identified in the coronal sections (**Fig. 1**). After filtering the number of differentially expressed genes (DEGs; FDR < 0.001, log2fold-change > |0.2|), we found that the hippocampal region had the greatest number of significant DEGs affected by sleep loss (592 DEGs), followed by the neocortex (401 DEGs), the hypothalamus (266 DEGs), and the thalamus (113 DEGs) (**Fig. 2A**). Some of these DEGs, such as *Rbm3*, *Hspa5* and *Srsf5*, have been previously shown to be affected after sleep deprivation in our previous studies of the hippocampus[11,35,36] and in studies of other brain regions[13–15,17,21,33,37,38].

The molecular functions of the DEGs showed region-specific differences (**Fig. 2B-E**). For the hippocampal region, many molecular functions related to RNA processing were enriched (**Fig. 2B**). For the neocortex, molecular functions related to protein kinase activity, GTPase activity, ubiquitin ligase activity, and DNA-binding transcription factor binding were enriched (**Fig. 2C**). The DEGs in the hypothalamus were enriched for molecular functions related to neuropeptide and hormone activity, as well as glutathione transferase and peroxidase activity (**Fig. 2D**). Finally, the DEGs in the thalamus were enriched for the Myogenic Regulatory Factor (MRF) binding molecular function (**Fig. 2E**). Surprisingly, ~98% of the DEGs in the hippocampal region were significantly downregulated whereas ~96% of the DEGs in the neocortex were significantly upregulated (**Fig. 2B-C**).

We next investigated how many of those total DEGs are uniquely affected in each brain region by analyzing the degree of overlap between the DEGs in the brain regions that had at least 50 DEGs affected by sleep deprivation (**Fig. 2F**). Although there were many connections between

different brain regions, the majority (50-83%) of the DEGs were specifically affected in their respective brain region. Of the 592 DEGs found in the hippocampal region, 489 were exclusively affected in the hippocampal region (489/592 DEGs), 306/401 in the neocortex, 199/266 in the hypothalamus, 56/113 in the thalamus, and 33/66 in the striatum-like amygdalar nuclei.

Hippocampal subregions are differentially impacted by sleep deprivation.

As our results here and previous studies have demonstrated, the hippocampus is highly susceptible to the effects of acute sleep deprivation[11,13,24,35,36]. This brain region is comprised of several substructures—CA1, CA2, CA3, and the dentate gyrus (DG)—each with different functions in learning and memory[39–44]. We performed a deconvolution of the CA1 pyramidal layer and the dentate gyrus (DG) granule cell layer using a reference scRNA-seq whole hippocampus mouse dataset from the Allen Brain Atlas[45] (**Fig. 3A**) and were able to distinguish the areas CA2 and CA3 pyramidal layers based on spatial topography. Similarly, because the dendritic layers of CA1 are known to undergo structural changes following sleep deprivation[46–48], we also used spatial topography to define and include the stratum radiatum and oriens layers of CA1 in our analysis (**Fig. 3B**). Differential gene expression analysis in each hippocampal subregion revealed unique gene expression changes and molecular functions enriched that were specific to a subregion (**Fig. 3C**). Of the DEGs identified in each region, 51/62 DEGs were uniquely affected in CA1, 34/41 in DG, 53/61 in stratum radiatum, and 4/4 in stratum oriens. The CA1 pyramidal layer and stratum radiatum were most impacted by sleep deprivation, with the most DEGs and unique DEGs of the areas examined. Stratum radiatum had 53 unique DEGs enough to enrich the cyclin-dependent protein serine/threonine kinase activity, as well as the

pyramidal CA1 cells with their 51 unique DEGs that enriched the glutamate receptor binding. Interestingly, there were no genes significantly affected in the combined CA2 and CA3 pyramidal layers after sleep deprivation. This finding supports other observations that CA1 and the DG are impacted by sleep deprivation while area CA3 is less affected[36,48].

Sleep deprivation causes layer-specific transcriptional changes in the cortex

The neocortex was the second-most impacted by sleep deprivation (**Fig. 2A**). The cortex comprises of different layers that each are involved in various functions of receiving, integrating, and outputting information[49]. To understand how sleep deprivation differently impacts the layers of the cortex, we examined the gene expression profiles within each cortical layer. We performed a deconvolution of the spatial datasets by integrating them with a reference scRNA-seq dataset of ~14,000 adult mouse cortical cell taxonomy from the Allen Institute[50]. This allowed us to identify the layers of the neocortex based on the prediction score in each spot (**Fig. 4A**) and perform differential gene expression analyses in each layer. Layers 2/3 and 5 are the most transcriptionally affected after sleep deprivation with 222 and 225 significant DEGs, respectively. Differential gene expression analysis in each cortical layer revealed distinct gene expression changes and molecular functions that were uniquely enriched in certain layers (**Fig. 4B**), which may relate to the differential function of these layers in intracortical processing and cortical output. Layer 5, which contains neurons that are the main output of the cortex, had 174 unique DEGs that included molecular functions related to sterol binding, cyclic adenosine monophosphate (cAMP) binding, structural constituent of postsynapse, and ion channel regulator activity. Layer 2/3, which functions largely in information processing within the cortex, had 149 unique DEGs that included molecular functions related to phosphatase inhibitor activity,

adenylate cyclase inhibiting G protein-coupled glutamate receptor activity, and ionotropic glutamate receptor binding.

Registration of Visium slices to a common anatomical reference space via the Spatial Transcriptomics Analysis Tool (STAnly) allows the unrestricted analysis of transcriptomic data across entire brain slices

Our deconvolution approach (used in **Fig. 4**) subdivides a given brain slice into different larger brain regions based on their transcriptomic activity. Although this is a powerful tool to analyze spatial gene expression changes, it inevitably comes at the price of a loss of spatial resolution, as this approach necessarily pools over larger brain regions, and requires a prior biological knowledge of cell type-specific gene expression profiles. To address this loss of spatial resolution, we established a new analysis tool (Spatial Transcriptomics ANaLYsis (STANLY) that aligns dots from multiple samples from different animals into one common anatomical reference space, the Common Coordinate Framework (CCF) of the Allen Mouse Brain Atlas, thus allowing a dot-by-dot comparison of the transcriptome in an unrestricted inference space (**Fig. 5A**). To account for different numbers of Visium spots across slices, we generated 'digital spots' in this same coordinate system to allow a statistical comparison across. Using this method, we detected at least 18,893 genes in all sample slices for changes in expression between NSD and SD. Of these, 428 genes were significantly differentially expressed, with 150 genes showing an upregulation in all significant spots, 22 showing downregulation in all significant spots, and 256 showing a combination of up and down regulation across the sample space. These DEGs include previously described upregulated genes like *Per1* **(Fig. 5B)**, *Nr4a1* **(Fig. 5C)**, *Homer1* **(Fig. 5D)**, and *Arc* **(Fig. 5E)**, which showed localized increases in the neocortex, as well as

downregulated genes like *Rbm3* **(Fig. 5F)** and *Cirbp* **(Fig. 5G)**, which showed hippocampal specific changes, similar to those seen in our deconvolution approach. Using ToppGene[51], we found the top five enriched mouse phenotypes were related to abnormal synaptic transmission (83 DEGs), abnormal synaptic physiology (83 DEGs), abnormal learning/memory/conditioning (84 DEGs), abnormal cognition (84 DEGs), and abnormal CNS synaptic transmission (75 DEGs) across the whole coronal slice. GO-molecular function (GO:MF) enrichment analysis showed similar functions enriched in previously identified brain region such as RNA binding (found in the hippocampus), Ubiquitin-like protein ligase activity, GTP binding, kinase activity (found in the neocortex), and neuropeptide and hormone activity (found in the hypothalamus) (**Fig. 3**).

Discussion

The identification of cell-type specific transcriptomic signatures has been invaluable in distinguishing subclasses of cell types in the brain[52] and has provided novel insights into brain disorders such as epilepsy, autism, Alzheimer's disease[53–55]. However, the lack of spatial information associated with single cell transcriptomics represents a significant obstacle[56,57] especially in an organ as complex as the brain. Spatial transcriptomics, using the Visium platform, combines a spatial barcode of RNA transcripts with near single cell sequencing resolution providing a major advance for understanding gene regulation across brain regions. However, the recent development of this technology means that it is largely untested for the analysis of differential gene expression. Here, we used this technique to examine the important problem of how acute sleep deprivation affects gene expression across brain regions. The effects of sleep deprivation on public health, and as a risk factor increasing the susceptibility and

incidence of numerous diseases, necessitate that we utilize and develop techniques that will provide more detailed understanding of the consequences of sleep loss.

The Visium spatial transcriptomic platform provided sequencing depth comparable to single cell and single nuclear transcriptomic studies in terms of gene number per spot, with the advantage of enriching mature RNA transcripts. Potentially, the clustering of a small number of cells in the spots of the Visium platform allows for a greater sequencing of mature cytoplasmic RNA molecules, compared to the nuclear mRNA that contains immature RNAs still being processed.

This technique allowed us to anatomically distinguish individual brain regions by aligning brain regions with the reference mouse Allen brain atlas, where we found that individual brain regions showed distinct transcriptional profiles after acute sleep deprivation. Individual cell types clustered within a brain region similar to single cell transcriptomic studies (**Fig. 1**). Thus, these results demonstrate the comparability of spatial transcriptomics to the resolution of single-cell approaches with the added power of simultaneous brain-wide investigation and additional spatial information.

Given the recent development of the spatial transcriptomics platform, we employed both a relatively large number of samples for a transcriptomics study and a highly conservative statistical analysis using an FDR of 0.001 to determine differential gene expression in individual brain regions following acute sleep deprivation. Importantly, all samples were collected at the same time of day as the circadian clock has independent effects on transcription[58,59]. We found that acute sleep deprivation had the greatest impact on gene regulation in the hippocampus, neocortex, hypothalamus and thalamus (**Fig. 2A**). Interestingly, this conservative approach strongly illustrated heterogeneity of brain regions in response to sleep deprivation, as we found little overlap in the differentially expressed genes across brain regions (**Fig. 2F**). Moreover, our

results conclusively demonstrate that directional changes in gene expression following acute sleep deprivation vary widely across brain regions; approximately 98% of the differentially expressed genes downregulated in the hippocampus, while the opposite was true in the neocortex, which had approximately 96% of the differentially expressed genes upregulated (**Fig. 2B, C**). Thus, analysis of gene expression changes after acute sleep deprivation in older studies, in which the entire forebrain was collected, may have masked the nuanced effects of sleep deprivation on gene regulation. The dramatic differences in gene expression across brain regions in response to sleep deprivation also suggests that a single theory to explain the impact of wakefulness on the brain or the function of sleep is unlikely to be satisfactory.

The work presented here establishes the robustness and fidelity of spatial transcriptomics for the determination and analysis of differential gene expression within brain subregions as well as for comparisons of gene expression across the brain. For example, in the hippocampus, we found that acute sleep deprivation significantly reduced gene expression involved in RNA processing similar to what was found in previous research[11]. In the neocortex, upregulation was observed for genes involved in DNA binding and transcription factor activity, protein kinase regulation, GTPase regulation and ubiquitin like protein ligase activity. This upregulation of genes involved in DNA binding and transcription factor activity, such as the transcription factor *Nr4a1*, may explain the greater percentage of upregulated genes found in the neocortex as increased expression of NR4A1 would lead to increased expression of its target genes. Although a smaller number of genes were identified in the hypothalamus and thalamus, they nonetheless indicate significant changes in molecular function[17]. For instance, we found that the most significant alterations in the hypothalamus were for genes associated with neuropeptide and hormone

signaling. The differences in the functions and molecular pathways affected in each region may provide key insights into how each structure is related to some of the broader and longer lasting effects of acute sleep deprivation. Importantly, the differentially expressed gene functions we identified in each brain region are consistent with the behavioral effects that have been observed following sleep deprivation and attributed to changes in neuronal function, such as changes in circadian behavior or impairments in long-term memory.

The high density of individually coded spots on the Visium slide grid enabled sub-regional analysis of gene expression between slices from sleep deprived and non-sleep deprived mice when combined with a deconvolution approach using single cell reference data sets from the Allen Brain Atlas for the hippocampus (**Fig. 3A**) and the cortex (**Fig. 4A**). Subregional analysis of the hippocampus was done for the CA1, CA2/3 pyramidal cell layers, dentate gyrus granule cell layer, and the stratum oriens and the stratum radiatum which contain diverse populations of interneurons. Although both the stratum oriens and the stratum radiatum contain interneurons, the functions of these two layers are distinct, and receive different anatomical inputs. Given the disparate functions and circuitry of the hippocampal subregions, we predicted that sleep deprivation would result in distinct transcriptional profiles in these subregions. We found that sleep deprivation induced the largest number of changes in gene expression in the CA1 and stratum radiatum. Surprisingly, there were only four genes affected by sleep deprivation in the stratum oriens, although interneurons within this region have been shown to be plastic and provide input to CA1 pyramidal cells[60]. These results suggest that sleep deprivation has the broadest impact on gene regulation in the excitatory neurons of the hippocampus. This result is consistent with previous research in which manipulations of protein synthesis within

hippocampal excitatory neurons ameliorated the impacts of sleep deprivation on hippocampus dependent long-term spatial memory[61]. However, it should be noted that the power of subregional analysis for differential gene expression within the hippocampus may be limited by the number of spots in each subregion. In comparison to the individual layered analysis of the neocortex, there were fewer differentially expressed genes detected in the subregions of the hippocampus (**Fig. 3C vs 4B**). However, future research in which single-cell RNA-seq is combined with spatial transcriptomics could resolve these issues.

We found that within the neocortex, sleep deprivation differentially affected individual cortical layers (**Fig. 4B**), and that Layers 2/3 and 5 were the most affected by sleep deprivation. Interestingly, changes in gene expression following sleep deprivation were unique for individual layers: more than 65% of the genes were unique in Layer 5 and 75% of the genes in Layer 2/3 were unique. Although the number of genes affected was smaller for Layer 4 and Layer 6, the number of layer specific gene changes for these layers was still approximately 50%. From this we can observe that there are distinct impacts of sleep deprivation on individual cortical layers. Indeed, Layer 2/3 function as corticocortical projections to layer 5 and form a prominent interlaminar pathway to amplify, integrate, distribute and temporarily store information within subsets of neurons[62]. From the Layer 5, pyramidal tract neurons project to multiple targets including ipsilateral striatum, thalamus, subthalamic nucleus and many brainstem and spinal cord regions[63]. The elevated level of response from these two layers highlight how the cortex is adapting in response to sleep deprivation, and these connections may better illustrate why cortical functions and properties are so altered by sleep loss[64].

Spatial transcriptomics provides a potentially powerful approach for large scale comparisons of gene expression across multiple conditions or disease states. For the full capability of spatial transcriptomics to be realized, it is necessary to develop the analysis tools for the alignment of spatial transcriptomic data sets into a common anatomical reference space to allow an unrestricted comparison of gene expression between samples. To further this goal, we pioneered the adaption of bioinformatic tools to facilitate the transformation and registration of spatial transcriptomic data sets with the anatomical reference space of the Allen Mouse Brain Atlas (**Fig. 5**). By computationally aligning the spatial transcriptomic data through a digital spot workflow with the Common Coordinate Framework, we can observe gene expression changes between the sleep deprived and non-sleep deprived conditions for individual genes of interest. This coordinate approach allows significant changes in gene expression to be visualized and analyzed for individual spots across the brain (**Fig.** 5) in greater detail and with much higher sensitivity for localized changes within larger anatomical structures than the region of interest approach above. We used this approach at its most basic level to examine single gene expression across the brain, finding 428 genes that significantly changed after sleep deprivation. However, our data shows that even genes with robust changes after sleep deprivation display regional differences in expression, which emphasizes that sleep deprivation has localized impacts on gene regulation. With the formidable technological advances that have been made over the past decade, specifically those enabling detailed analysis of gene regulation at multiple levels, one of the greatest challenges facing neuroscientists is the integration and management of complex multimodal data sets. There is a critical need to integrate large data sets for spatial and specific cell type characterization of the mouse brain, as the majority of preclinical research is done using the mouse model. The bioinformatic approach for spatial gene expression analysis across brain

337 regions that we developed for this study helps to meet the challenge of integrating complex data
338 sets for mouse spatial transcriptomic data sets and reveals critical regional selectivity in the
339 impact of brief periods of sleep loss across the brain.

340 Material and Methods

341 ***Animals***: Male C57BL/6J mice (Jackson Laboratory #000664), age 2.5-3.5 months were used for
342 all the experiments. Mice were group housed (up to 5 per cage) in cages containing soft bedding
343 with food (NIH-31, irradiated modified mouse diet, #7913) and water available *ad libitum* in a
344 12hr :12hr light-dark schedule. The start of the lights-on period is defined as Zeitgeber time zero
345 (ZT 0). Experiments were conducted according to National Institutes of Health guidelines for
346 animal care and use and were approved by the Institutional Animal Care and Use Committee
347 (IACUC) at the University of Iowa.

348 ***Sleep deprivation***: All mice were single housed seven days prior to the experiment with corncob
349 bedding (Envigo, Teklad ¼" corncob, #7907) and soft bedding for nesting. Mice had *ad libitum*
350 access to food and water during sleep deprivation. All mice were habituated for 5 days prior to
351 the experiment by the researcher conducting the experiments. Habituation, performed in the
352 behavior room for experiments, was done by holding each mouse in the palm for 2 min and then
353 after returning to the home cage, tapping of the cage for 2. Sleep deprivation was performed for
354 5 hours from ZT 0 – ZT 5 using the gentle handling method[31,32]. Briefly, the experimenter tapped
355 the side of the cage, as needed, to keep each mouse awake. When taps were no longer sufficient
356 the mice received a light "cage shake" to rouse the animal. NSD mice remained in the colony
357 housing room throughout the 5-hour period.

Tissue processing and Visium data generation: Each mouse was rapidly euthanized by cervical dislocation at ZT 5 with the whole brain rapidly extracted and flash frozen by ≥ -70°C isopentane (n=8 SD and n=8 NSD). Frozen brains were stored at -80°C. Prior to sectioning, a small tissue sample from the cerebellum of each frozen brain was removed, RNA extracted and quality assessed using RNA Integrity Number (RIN). Brains with a RIN above 7 were embedded in optimal cutting temperature medium (OCT) and cryosectioned at -20 °C (10µm sections) with the Leica CM3050 S Cryostat in the Iowa Neuroscience Institute (INI) NeuroBank Core. One coronal section per mouse, corresponding approximately to section 45 of the Paxinos Mouse Brain atlas, was mounted on Visium Spatial Gene Expression Slides (catalog no. 2000233, 10x Genomics). Sections were immediately processed with the 10x Genomics Visium Gene Expression Slide kit. Full details on the methods used are found in the manufacturer's instructions (CG000239 Rev A User Guide Visium Spatial Gene Expression Reagent Kits). First, the slides were fixed in chilled methanol at -20˚C then stained with hematoxylin and eosin (H&E) to visualize the slices. Brightfield images of the H&E-stained sections were acquired (20X) using an Olympus BX61 Upright Microscope. Raw images were stitched together with the CellSens software (Version 3.2; Olympus) and exported as tiff files. Tissue was then permeabilized with Permeabilization Enzyme (provided by 10X Genomics in the Visium Gene Expression Slide & Reagent Kit, PN-1000184) for 18 min as determined based on tissue optimization time-course experiments. Permeabilization resulted in the release of polyA mRNA from the tissue enabling capture by poly(dT) primers precoated on the Visium Gene Expression slides. Slides also contained barcoded probes with unique molecular identifiers (UMI) so that the spatial gene distribution was mapped. After reverse transcription and second strand synthesis, the amplified cDNA samples from the Visium slides were transferred, purified, and quantified for

library preparation. Sequencing libraries were prepared by the Iowa Institute of Human Genetics (IIHG) Genomics Division, according to the Visium Spatial Gene Expression User Guide. Libraries were pooled for sequencing to achieve sequencing depth balance across the samples based on the relative area of coverage of each tissue on the slide. The fragmented cDNA pools were sequenced using an Illumina NovaSeq 6000 SP or S1 flowcell running 100 cycle SBS chemistry v1.5 and aimed for 200 million total read pairs. Read 1 was 48 nucleotide length (10 nt i5 index + 10 nt i7 index + 28 nt Spatial Barcode, UMI) and read 2 was 90 nucleotides length (insert).

Visium data processing: Raw FASTQ files and histology images were processed with the Space Ranger software v.1.3.1, which uses STAR v.2.7.10a for genome alignment against the Cell Ranger mm10 reference genome refdata-gex-mm10-2020-A, available at: https://cf.10xgenomics.com/supp/spatial-exp/refdata-gex-mm10-2020-A.tar.gz. Quantification and statistical analysis were done with Partek Flow package (Build version 10.0.21.0621) in the Iowa Institute of Human Genetics (IIHG) Genomics Division. Briefly, to avoid raw gene expression counts of 0, a value of 0.001 was added to all counts prior to running SCTransform for normalization and scaling steps. Interpretation of spatial transcriptomic data requires effective preprocessing and normalization to remove spot-to-spot technical variability such as the number of molecules detected in each spot, which can confound biological heterogeneity with technical effects. Recently, a new modeling framework for normalization and variance stabilization of molecular count data was made available for spatial datasets which improves downstream analytical tasks including gene selection, dimensional reduction, and differential expression[65] from spatial datasets. After applying this modeling framework, the dimensionality of each sample was reduced using 100 principal components from the variance of the features.

Then, an unbiased graph-based clustering was performed to identify the transcriptional signatures of each spot using the Louvain clustering algorithm that includes 30 nearest neighbors and 20 principal components. This threshold of 20 principal components was chosen based the elbow plot of each sample where most of the transcriptional variation was captured within the first 20 principal components. Since SCTransform is not suitable for differential gene expression analyses, output data from Space Ranger were renormalized with a more classical approach including Counts Per Million (each gene's raw read count in a sample divided by the total number of counts per million in a sample), with a value of 1 added to avoid 0 counts and errors in differential analysis, and finally a log base 2 transformation applied to all values to model and measure proportional fold changes. This normalization revealed similar counts variation across samples. The cluster and brain region labels previously computed by the SCTransform algorithm were then transferred to this log-transformed data. Differential gene expression analysis was performed using the non-parametric Kruskal-Wallis rank sum test because the distribution of the counts does not conform to a normal or binomial distribution. Rank-sum tests have been the most widely used approach in the field of single-cell transcriptomics[66] because it is assumed that every cell (or spot for spatial transcriptomics) is an identical replicate that defines the sample size of the statistics and this approach generates fewer false positives. In this study, the Kruskal-Wallis test was able to assign a median count of 1 (or 0 in log2), for both conditions, for a gene that is not expressed in a given brain region resulting in a fold change of 1 (or 0 in log2). Therefore, a gene was considered significantly differentially expressed (DE) if it has a false discovery rate (FDR) step-up (p-value adjusted) below 0.001 and a log2fold-change $\geq |0.2|$.

Deconvolution: integration with single-cell data: At 55µm, spots from the Visium assay encompass the expression profiles of 10-20 cells and represent averaged expression of the

heterogeneous mixture of cells at the spot level. For this reason, computational techniques called deconvolution have been developed that use scRNA-seq data to infer cell proportions in bulk transcriptomic samples[67]. Consequently, deconvolution of each of the spatial voxels was performed to predict the underlying composition of cell types. We used a reference scRNA-seq dataset of ~14,000 adult mouse cortical cell taxonomy from the Allen Institute[50]. We applied the anchor-based integration that enables the probabilistic transfer of annotations from a reference to a query set, here it is our SCTransformed gene expression matrix output from Partek Flow®. We then took advantage of the SCTransform normalization to label transfer the cell-type identification of scRNA-seq clusters into the transcriptional signatures of the spatial voxels. The voxels with the highest prediction score were labeled and transferred to the log-transformed data for downstream differential gene expression analysis.

GO molecular function enrichment analyses of differentially expressed genes (DEGs): The ClueGO[68] and CluePedia[69] plug-ins of the Cytoscape 3.9.0 software[70] were used in "Functional analysis" mode for analyzing the Gene Ontology Molecular Function (4691 terms) database in networks for DEGs. The names of significant DEGs were pasted into the "Load Marker List" of ClueGO, and the organism "Mus Musculus [10090]" was selected. Only pathways with a p-value < 0.05 were displayed on the figures. The GO Term Fusion was used allowing for the fusion of GO parent-child terms based on similar associated genes. The GO Term Connectivity had a kappa score of 0.4. The enrichment was performed using a two-sided hypergeometric test. The p-values were corrected with a Bonferroni step down approach.

Data and spot preprocessing for STANLY: We inspected all 16 samples visually, excluding any with serious tissue damage or a large amount of tissue folding after adhesion to the slide limiting our analysis to 13 samples. Samples were collected from the left or right hemisphere, but to

maximize spatial similarity, we mirrored the right hemisphere samples (2) to the left hemisphere, so that all samples could be aligned in the left hemisphere space. After importing the image data of the Visium slice along with the filtered feature matrix we reduced the list of spots per slice down to only those listed as "in tissue" by Space Ranger and masked the filtered feature matrix for each sample to first remove empty non-tissue spots. We further removed from the analysis any in tissue spots that had fewer than 5,000 total gene counts, which might indicate an error with the spot itself. Any genes that expressed 0 total reads across an entire sample were removed due to low statistical viability. For these 13 samples the average number of in tissue spots per slide was 2548. Given the localized nature of gene expression to certain tissues or regions of a sample, raw gene counts in each spot are likely to be correlated to their neighbors, but not necessarily across an entire sample. This leads to a high likelihood of a right tail distribution of data when genes are regionally expressed, with potentially high counts in some spots and counts of zero in others. In order to account for this distribution of data we performed log base 2 normalization on the raw gene counts being fed into the analysis. Log base2 normalization is specifically useful in the case of biological data such as gene counts as this normalizes the data to look for proportional rather than additive changes in expression.

Image preprocessing: Our data was collected as coronal slices of the mouse brain, chosen to be similar to slice 45 in the Paxinos Mouse Atlas, which is similar to Allen Brain Atlas slice 70, so as a template we chose slice 70 from the Allen Common Coordinate Framework[30]. The code base for image preprocessing steps were performed using SimpleITK[71] (v.5.3.0) and scikit-image[72] (v.0.19.3) as well as SciPy[73] (v.1.7.3) and NumPy[74] (v.1.21.5) for processing the filtered feature matrices from Space Ranger and performing analysis on the registered spots.

For our current pipeline, most coronal tissue adhered to the slide in such a way that a simple rotation of [0°, 90°, 180, or 270°] is sufficient to bring the tissue images into the same general orientation as the template image. For those images from right hemisphere, we additionally performed a symmetrical flip on the images and their corresponding spots to match the hemisphere of the template image. This hemisphere combination allows us to maximize the usability of tissue slices in the analysis. Any rotation or mirroring transformation to the tissue image is applied also to the spot coordinates so that these maintain the same space throughout processing. One common problem when trying to register different image modalities is how to handle differences in voxel resolution. In the case of Visium, we know the size of each spot (55µm) as well as their distance on center from each other (100µm). Using the image spot scaling information provided by Space Ranger we are able to accurately calculate the size of each spot in the original high-resolution image and calculate the voxel to real world resolution and bring the image into the same resolution as the template. In order to perform the registration, the tissue image is converted to gray scale. The template image is also min-max normalized in order to bring it into range of a normal gray scale image rather than the original multi-channel image. In order to mask the background noise from the sample images we ran a 20µm Gaussian blur on each image, from which we generated a binary tissue mask using the Otsu method, which allows us to mask out all voxels except for those that contain tissue from the registration process.

Image Registration: After the initial rotation, we selected a single image from our sample set to act as our “best fit.” For the best fit we chose a sample that had good shape and image quality. This selection of a best fit image is done to minimize the need of registering each sample

individually to the template image, which has a higher potential for error, and instead register them all to the best fit image that shares more of the image characteristics of H&E stains. To run the registration of the best fit sample (**Fig. 5A$_1$**) and its spots (**Fig. 5A$_2$**) to the CCF template image (**Fig. 5A$_3$**) we used the symmetric image normalization method (SyN) nonlinear registration tools from Advanced Normalization Tools (ANTs)[75] (v.2.3.2), specifically the SyNAggro transformation using a mattes SyN metric with parameters of: SyN sampling=32, flow sigma=3, gradient step=0.1, and registration iterations=[120, 100,80,60,40,20,0]. The result of this registration can be seen applied to the tissue image (**Fig. 5A$_4$**) and to the tissue spots (**Fig. 5A$_5$**). After the best fit image was registered to the CCF template image we used the same registration parameters to register the remaining samples to the unregistered best fit image, and then finally applied "best fit to template" transformation generated above to each sample and its spots, bringing them into common space (**Fig. 5A$_6$**).

Digital Spots: With all sample images and their spot coordinates in the CCF reference space, we developed a method to create "digital spots" to make running analysis on multiple samples simpler and more closely representative of spacing of the spots in relation to each other. Visium spots are organized in a honeycomb arrangement, where each 55µm spot has 6 equidistant nearest neighbors spaced 100µm away on center. Knowing this, we created digital spots that replicate the characteristics of the Visium spots in the digital space. Using the 10µm resolution of the CCF template, we wrote a function that generated a honeycomb spaced grid of digital spots in CCF space and within the bounds of our template mask by defining the desired spacing between digital spots. Due to inevitable spatial uncertainty during registration, we set the spot spacing of our digital sampling to 150µm in order to "smooth" the data, a method already common in neuroimaging. We then measured Euclidean distance between each digital spot and

template registered tissue coordinates from all samples in the experiment. We sorted these distances and selected at each digital spot from each sample the 7 nearest neighbor spots up to 450µm, or approximately 3 digital spots away from the center of the digital spot. We chose 7 because of the hexagonal properties of the spot spacing, with every 1 spot having 6 nearest neighbors. Each digital spot is therefore a vector of multiple spots from each of the registered samples, e.g. for our 13 samples, this sampling would include up to 7 x 13 sample spots at each digital spot. For our data, this method generated 2,052 spots for the CCF template image (**Fig. 5A7**), of which we removed 160 spots from analysis for not having sufficient nearest neighbors across samples, leaving 1,892 spots. Examples of this sampling can be seen in **Fig. 5B-G**, with the first image in each plot showing the mean of the digital spots of log base 2 normalized gene counts for NSD samples (**Fig. 5B$_1$-G$_1$**), the second image showing the mean of normalized gene counts for SD (**Fig. 5B$_2$-G$_2$**).

Statistical analysis of digital spots: We performed a two-tailed t-test on each digital spot with a Šidák p-value correction (Šidák, 1967) for the number of digital spots as follows:

$$\alpha_s = 1 - (1 - \alpha)^{(1/m)}$$

Where α_s is the Šidák corrected p-value, α is the original p-value (e.g. 0.05 or 0.01) and m is the number of digital spots used in the analysis. The number of digital spots is determined by the distance between spots and the actual size of the slice used to create the digital spots. In our case, with a digital smoothed spot distance of 150µm the number of digital spots came to 2,052, as compared to the mean of 2,538.46 spots across our sample slices with a spot distance of

100µm. Based on these numbers, any genes that differed between NSD and SD with a p-value < 2.50e-05 for at least 3 of the 1,892 digital spots present in all samples was considered significantly differentially expressed. The results of the two-tailed t-test for 6 example DEGs can be found in figure 5 (**Fig. 5B$_3$-G$_3$**).

Functional enrichment analysis of DEGs using ToppGene: ToppFun, the functional enrichment analysis tool from ToppGene suite[51] was run by pasting the list of 428 DEGs generated by STANLY into the ToppFun enrichment gene set and searching for an enrichment of GO: Molecular Functions, GO: Biological Processes, and Mouse Phenotypes.

References

1. Wheaton, A. G., Jones, S. E., Cooper, A. C. & Croft, J. B. Short Sleep Duration Among Middle School and High School Students — United States, 2015. *Morb. Mortal. Wkly. Rep.* **67**, 85–90 (2018).
2. McHill, A. W. & Wright, K. P. Role of sleep and circadian disruption on energy expenditure and in metabolic predisposition to human obesity and metabolic disease. *Obes. Rev. Off. J. Int. Assoc. Study Obes.* **18 Suppl 1**, 15–24 (2017).
3. Hudson, A. N., Van Dongen, H. P. A. & Honn, K. A. Sleep deprivation, vigilant attention, and brain function: a review. *Neuropsychopharmacol. Off. Publ. Am. Coll. Neuropsychopharmacol.* **45**, 21–30 (2020).
4. Krause, A. J. *et al.* The sleep-deprived human brain. *Nat. Rev. Neurosci.* **18**, 404–418 (2017).
5. Raven, F., Van der Zee, E. A., Meerlo, P. & Havekes, R. The role of sleep in regulating structural plasticity and synaptic strength: Implications for memory and cognitive function. *Sleep Med. Rev.* **39**, 3–11 (2018).
6. Sabia, S. *et al.* Association of sleep duration in middle and old age with incidence of dementia. *Nat. Commun.* **12**, 2289 (2021).
7. Shi, L. *et al.* Sleep disturbances increase the risk of dementia: A systematic review and meta-analysis. *Sleep Med. Rev.* **40**, 4–16 (2018).
8. Wang, C. & Holtzman, D. M. Bidirectional relationship between sleep and Alzheimer's disease: role of amyloid, tau, and other factors. *Neuropsychopharmacology* **45**, 104–120 (2020).

9. Wu, H., Dunnett, S., Ho, Y.-S. & Chang, R. C.-C. The role of sleep deprivation and circadian rhythm disruption as risk factors of Alzheimer's disease. *Front. Neuroendocrinol.* **54**, 100764 (2019).

10. Musiek, E. S. & Holtzman, D. M. Mechanisms linking circadian clocks, sleep, and neurodegeneration. *Science* **354**, 1004–1008 (2016).

11. Gaine, M. E. *et al.* Altered hippocampal transcriptome dynamics following sleep deprivation. *Mol. Brain* **14**, 125 (2021).

12. Nilsson, E. K., Boström, A. E., Mwinyi, J. & Schiöth, H. B. Epigenomics of Total Acute Sleep Deprivation in Relation to Genome-Wide DNA Methylation Profiles and RNA Expression. *OMICS J. Integr. Biol.* **20**, 334–342 (2016).

13. Vecsey, C. G. *et al.* Genomic analysis of sleep deprivation reveals translational regulation in the hippocampus. *Physiol. Genomics* **44**, 981–991 (2012).

14. Cirelli, C. & Tononi, G. Gene expression in the brain across the sleep–waking cycle. *Brain Res.* **885**, 303–321 (2000).

15. Cirelli, C., Gutierrez, C. M. & Tononi, G. Extensive and Divergent Effects of Sleep and Wakefulness on Brain Gene Expression. *Neuron* **41**, 35–43 (2004).

16. Cirelli, C. Cellular consequences of sleep deprivation in the brain. *Sleep Med. Rev.* **10**, 307–321 (2006).

17. Mackiewicz, M. *et al.* Macromolecule biosynthesis: a key function of sleep. *Physiol. Genomics* **31**, 441–457 (2007).

18. Mongrain, V., Spada, F. L., Curie, T. & Franken, P. Sleep Loss Reduces the DNA-Binding of BMAL1, CLOCK, and NPAS2 to Specific Clock Genes in the Mouse Cerebral Cortex. *PLOS ONE* **6**, e26622 (2011).

19. Cirelli, C. & Tononi, G. Differential expression of plasticity-related genes in waking and sleep and their regulation by the noradrenergic system. *J. Neurosci. Off. J. Soc. Neurosci.* **20**, 9187–9194 (2000).

20. Scarpa, J. R. *et al.* Cross-species systems analysis identifies gene networks differentially altered by sleep loss and depression. *Sci. Adv.* **4**, eaat1294 (2018).

21. Gerstner, J. R. *et al.* Removal of unwanted variation reveals novel patterns of gene expression linked to sleep homeostasis in murine cortex. *BMC Genomics* **17**, 727 (2016).

22. Hor, C. N. *et al.* Sleep–wake-driven and circadian contributions to daily rhythms in gene expression and chromatin accessibility in the murine cortex. *Proc. Natl. Acad. Sci.* **116**, 25773–25783 (2019).

23. Delorme, J. *et al.* Sleep loss drives acetylcholine- and somatostatin interneuron–mediated gating of hippocampal activity to inhibit memory consolidation. *Proc. Natl. Acad. Sci.* **118**, e2019318118 (2021).

24. Delorme, J. *et al.* Hippocampal neurons' cytosolic and membrane-bound ribosomal transcript profiles are differentially regulated by learning and subsequent sleep. *Proc. Natl. Acad. Sci. U. S. A.* **118**, e2108534118 (2021).

25. Method of the Year 2020: spatially resolved transcriptomics. *Nat. Methods* **18**, 1–1 (2021).

26. Maynard, K. R. *et al.* Transcriptome-scale spatial gene expression in the human dorsolateral prefrontal cortex. *Nat. Neurosci.* **24**, 425–436 (2021).

27. Dixon, E. E., Wu, H., Muto, Y., Wilson, P. C. & Humphreys, B. D. Spatially Resolved Transcriptomic Analysis of Acute Kidney Injury in a Female Murine Model. *J. Am. Soc. Nephrol.* **33**, 279–289 (2022).

617 28. Nerurkar, S. N. *et al.* Transcriptional Spatial Profiling of Cancer Tissues in the Era of
618 Immunotherapy: The Potential and Promise. *Cancers* **12**, 2572 (2020).
619 29. He, B. *et al.* Integrating spatial gene expression and breast tumour morphology via deep
620 learning. *Nat. Biomed. Eng.* **4**, 827–834 (2020).
621 30. Wang, Q. *et al.* The Allen Mouse Brain Common Coordinate Framework: A 3D
622 Reference Atlas. *Cell* **181**, 936-953.e20 (2020).
623 31. Graves, L. A., Heller, E. A., Pack, A. I. & Abel, T. Sleep Deprivation Selectively Impairs
624 Memory Consolidation for Contextual Fear Conditioning. *Learn. Mem.* **10**, 168–176 (2003).
625 32. Prince, T.-M. *et al.* Sleep deprivation during a specific 3-hour time window post-training
626 impairs hippocampal synaptic plasticity and memory. *Neurobiol. Learn. Mem.* **109**, 122–130
627 (2014).
628 33. Terao, A., Greco, M. A., Davis, R. W., Heller, H. C. & Kilduff, T. S. Region-specific
629 changes in immediate early gene expression in response to sleep deprivation and recovery
630 sleep in the mouse brain. *Neuroscience* **120**, 1115–1124 (2003).
631 34. Puentes-Mestril, C. *et al.* Sleep Loss Drives Brain Region-Specific and Cell Type-
632 Specific Alterations in Ribosome-Associated Transcripts Involved in Synaptic Plasticity and
633 Cellular Timekeeping. *J. Neurosci. Off. J. Soc. Neurosci.* **41**, 5386–5398 (2021).
634 35. Lyons, L. C., Chatterjee, S., Vanrobaeys, Y., Gaine, M. E. & Abel, T. Translational
635 changes induced by acute sleep deprivation uncovered by TRAP-Seq. *Mol. Brain* **13**, (2020).
636 36. Vecsey, C. G. *et al.* Sleep deprivation impairs cAMP signalling in the hippocampus.
637 *Nature* **461**, 1122–1125 (2009).
638 37. Cirelli, C. & Tononi, G. Differences in gene expression between sleep and waking as
639 revealed by mRNA differential display. *Mol. Brain Res.* **56**, 293–305 (1998).

640 38. Thompson, C. *et al.* Molecular and Anatomical Signatures of Sleep Deprivation in the
641 Mouse Brain. *Front. Neurosci.* **4**, (2010).
642 39. Benoy, A., Dasgupta, A. & Sajikumar, S. Hippocampal area CA2: an emerging
643 modulatory gateway in the hippocampal circuit. *Exp. Brain Res.* **236**, 919–931 (2018).
644 40. Kesner, R. P. An analysis of dentate gyrus function (an update). *Behav. Brain Res.* **354**,
645 84–91 (2018).
646 41. Nakashiba, T. *et al.* Young Dentate Granule Cells Mediate Pattern Separation whereas
647 Old Granule Cells Contribute to Pattern Completion. *Cell* **149**, 188–201 (2012).
648 42. Nakazawa, K. *et al.* Requirement for Hippocampal CA3 NMDA Receptors in Associative
649 Memory Recall. *Science* **297**, 211–218 (2002).
650 43. Remondes, M. & Schuman, E. M. Role for a cortical input to hippocampal area CA1 in
651 the consolidation of a long-term memory. *Nature* **431**, 699–703 (2004).
652 44. Place, R. *et al.* NMDA signaling in CA1 mediates selectively the spatial component of
653 episodic memory. *Learn. Mem.* **19**, 164–169 (2012).
654 45. Yao, Z. *et al.* A taxonomy of transcriptomic cell types across the isocortex and
655 hippocampal formation. *Cell* **184**, 3222-3241.e26 (2021).
656 46. Bolsius, Y. G., Meerlo, P., Kas, M. J., Abel, T. & Havekes, R. Sleep deprivation reduces
657 the density of individual spine subtypes in a branch-specific fashion in CA1 neurons. *J. Sleep*
658 *Res.* **31**, e13438 (2022).
659 47. Spano, G. M. *et al.* Sleep Deprivation by Exposure to Novel Objects Increases Synapse
660 Density and Axon-Spine Interface in the Hippocampal CA1 Region of Adolescent Mice. *J.*
661 *Neurosci.* **39**, 6613–6625 (2019).

662 48. Havekes, R. *et al.* Sleep deprivation causes memory deficits by negatively impacting
663 neuronal connectivity in hippocampal area CA1. *eLife* **5**, e13424 (2016).
664 49. Shepherd, G. M. G. Corticostriatal connectivity and its role in disease. *Nat. Rev.*
665 *Neurosci.* **14**, 278–291 (2013).
666 50. Tasic, B. *et al.* Adult mouse cortical cell taxonomy revealed by single cell
667 transcriptomics. *Nat. Neurosci.* **19**, 335–346 (2016).
668 51. Chen, J., Bardes, E. E., Aronow, B. J. & Jegga, A. G. ToppGene Suite for gene list
669 enrichment analysis and candidate gene prioritization. *Nucleic Acids Res.* **37**, W305–W311
670 (2009).
671 52. Lake, B. B. *et al.* Neuronal subtypes and diversity revealed by single-nucleus RNA
672 sequencing of the human brain. *Science* **352**, 1586–1590 (2016).
673 53. Pfisterer, U. *et al.* Identification of epilepsy-associated neuronal subtypes and gene
674 expression underlying epileptogenesis. *Nat. Commun.* **11**, 5038 (2020).
675 54. Velmeshev, D. *et al.* Single-cell genomics identifies cell type–specific molecular changes
676 in autism. *Science* **364**, 685–689 (2019).
677 55. Murdock, M. H. & Tsai, L.-H. Insights into Alzheimer's disease from single-cell
678 genomic approaches. *Nat. Neurosci.* (2023) doi:10.1038/s41593-022-01222-2.
679 56. Kulkarni, A., Anderson, A. G., Merullo, D. P. & Konopka, G. Beyond bulk: a review of
680 single cell transcriptomics methodologies and applications. *Curr. Opin. Biotechnol.* **58**, 129–
681 136 (2019).
682 57. Saura, C. A., Deprada, A., Capilla-López, M. D. & Parra-Damas, A. Revealing cell
683 vulnerability in Alzheimer's disease by single-cell transcriptomics. *Semin. Cell Dev. Biol.*
684 **139**, 73–83 (2023).

685 58. Noya, S. B. *et al.* The forebrain synaptic transcriptome is organized by clocks but its
686 proteome is driven by sleep. *Science* **366**, eaav2642 (2019).
687 59. Brüning, F. *et al.* Sleep-wake cycles drive daily dynamics of synaptic phosphorylation.
688 *Science* **366**, eaav3617 (2019).
689 60. Le Duigou, C., Savary, E., Kullmann, D. M. & Miles, R. Induction of Anti-Hebbian LTP
690 in CA1 Stratum Oriens Interneurons: Interactions between Group I Metabotropic Glutamate
691 Receptors and M1 Muscarinic Receptors. *J. Neurosci. Off. J. Soc. Neurosci.* **35**, 13542–13554
692 (2015).

693 61. Tudor, J. C. *et al.* Sleep deprivation impairs memory by attenuating mTORC1-dependent
694 protein synthesis. *Sci. Signal.* **9**, ra41–ra41 (2016).
695 62. Brown, S. P. & Hestrin, S. Intracortical circuits of pyramidal neurons reflect their long-
696 range axonal targets. *Nature* **457**, 1133–1136 (2009).
697 63. Kita, T. & Kita, H. The Subthalamic Nucleus Is One of Multiple Innervation Sites for
698 Long-Range Corticofugal Axons: A Single-Axon Tracing Study in the Rat. *J. Neurosci.* **32**,
699 5990–5999 (2012).
700 64. Libedinsky, C. *et al.* Sleep Deprivation Alters Valuation Signals in the Ventromedial
701 Prefrontal Cortex. *Front. Behav. Neurosci.* **5**, (2011).
702 65. Hafemeister, C. & Satija, R. Normalization and variance stabilization of single-cell RNA-
703 seq data using regularized negative binomial regression. *Genome Biol.* **20**, 296 (2019).
704 66. Squair, J. W. *et al.* Confronting false discoveries in single-cell differential expression.
705 *Nat. Commun.* **12**, 5692 (2021).

67. Avila Cobos, F., Alquicira-Hernandez, J., Powell, J. E., Mestdagh, P. & De Preter, K. Benchmarking of cell type deconvolution pipelines for transcriptomics data. *Nat. Commun.* **11**, 5650 (2020).

68. Bindea, G. *et al.* ClueGO: a Cytoscape plug-in to decipher functionally grouped gene ontology and pathway annotation networks. *Bioinforma. Oxf. Engl.* **25**, 1091–1093 (2009).

69. Bindea, G., Galon, J. & Mlecnik, B. CluePedia Cytoscape plugin: pathway insights using integrated experimental and in silico data. *Bioinforma. Oxf. Engl.* **29**, 661–663 (2013).

70. Shannon, P. *et al.* Cytoscape: a software environment for integrated models of biomolecular interaction networks. *Genome Res.* **13**, 2498–2504 (2003).

71. Beare, R., Lowekamp, B. & Yaniv, Z. Image Segmentation, Registration and Characterization in R with SimpleITK. *J. Stat. Softw.* **86**, (2018).

72. Walt, S. van der *et al.* scikit-image: image processing in Python. *PeerJ* **2**, e453 (2014).

73. Virtanen, P. *et al.* SciPy 1.0: fundamental algorithms for scientific computing in Python. *Nat. Methods* **17**, 261–272 (2020).

74. Harris, C. R. *et al.* Array programming with NumPy. *Nature* **585**, 357–362 (2020).

75. Avants, B. B., Epstein, C. L., Grossman, M. & Gee, J. C. Symmetric diffeomorphic image registration with cross-correlation: Evaluating automated labeling of elderly and neurodegenerative brain. *Med. Image Anal.* **12**, 26–41 (2008).

Data availability

Data analysis and processing was performed using commercial code from Partek Flow package at https://www.partek.com/partek-flow/.

Acknowledgments

Funding resources, including Hensing Brain and Behavior Fund Carver Trust Fund (00-520-17-3410-20002-8-0491044-6210-850-00000-20-6735).

The study was supported by the National Institutes of Health R01 Grant (R01AG062398) to T.A. and L.C.L., the University of Iowa Hawkeye Intellectual and Developmental Disability Research Center (P50 HD 103556; L. Strathearn and T.A., multi-PIs), and the Hensing Brain and Behavior Fund Carver Trust Fund. T.A. is the Roy J. Carver Chair of Neuroscience.

The authors acknowledge Xiaowen Wang's exceptional technical support from Partek Inc., which was crucial for Visium spatial RNAseq data analysis.

Visium data presented herein were obtained at the Iowa NeuroBank Core in the Iowa Neuroscience Institute, and the Genomics Division in the Iowa Institute of Human Genetics which is supported, in part, by the University of Iowa Carver College of Medicine.

Author contributions

T.A. designed the study. E.N.W performed the sleep deprivation and tissue collection. LC. Lin performed the tissue preparation for 10x Genomics Visium Gene Expression. Y.V. and Z.P. performed the transcriptomic and statistical analysis with the advice and guidance of the senior authors. Y.V., Z.P., Lisa C.L., and E.N.W. wrote the manuscript with input from all the authors.

Competing interests

The authors declare no competing interests.

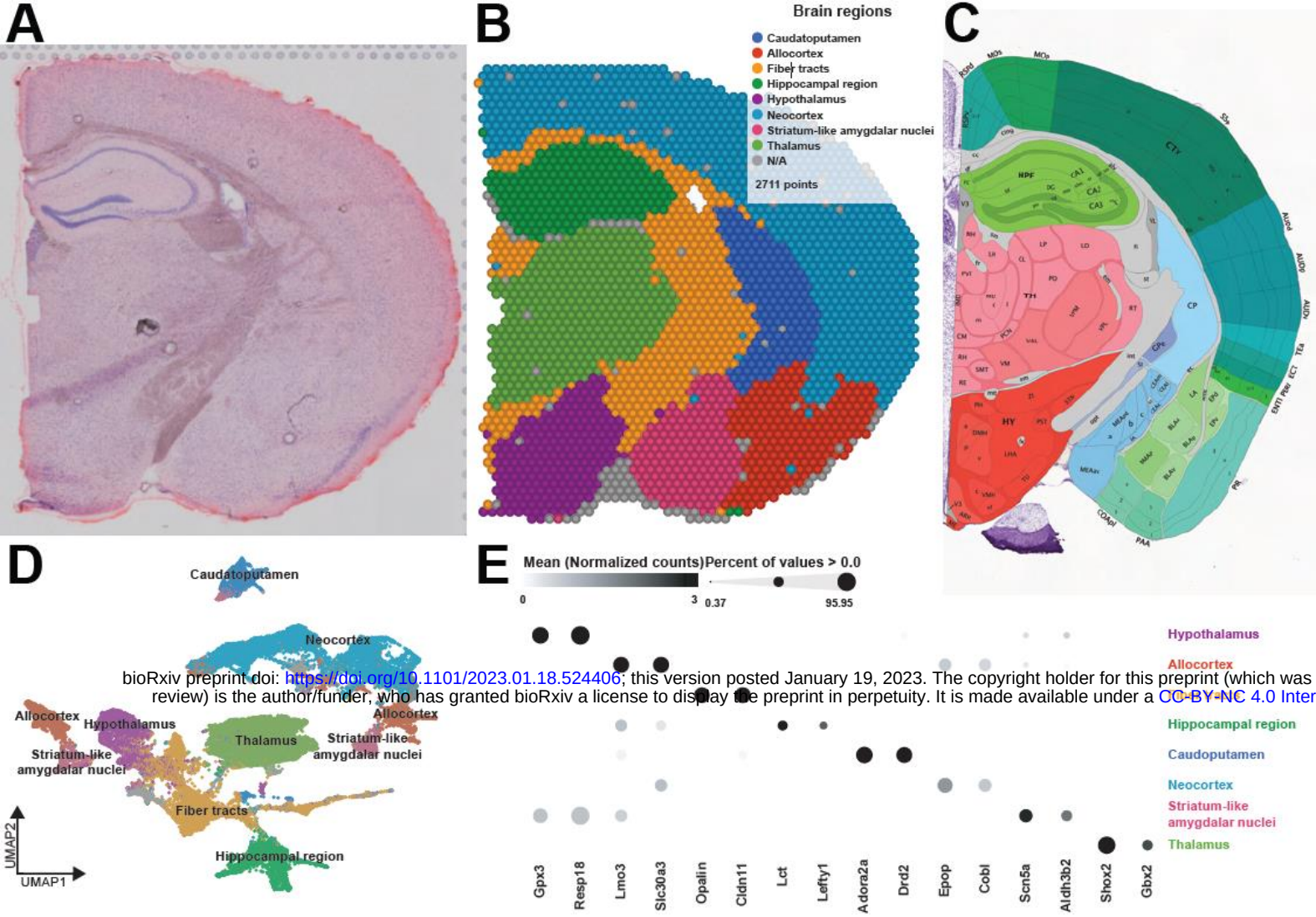

Figure 1. Spatial patterns of gene expression define anatomically distinct brain regions. A. Coronal tissue section H&E histology staining from sample 4. **B**. Graph-based cluster identification from spot-level (2,711 spots) of sample 4. Each spot is colored based on the transcriptional signature computed from 20 principal components using Louvain clustering algorithm. The brain regions are labeled in the colored legend. **C**. Screenshot of the reference mouse Allen brain atlas (coronal section image 72 of 132, position 285, http://atlas.brain-map.org/). **D**. UMAP plot based on the transcriptional signature of each spot. **E**. Bubble plot of the most significant computed biomarkers for each brain region. The bubble chart shows the expression level of biomarkers in each brain region. Bubble diameters are proportional to the percentage of spots that show expression of the biomarker. For each brain region, two significant biomarkers are displayed.

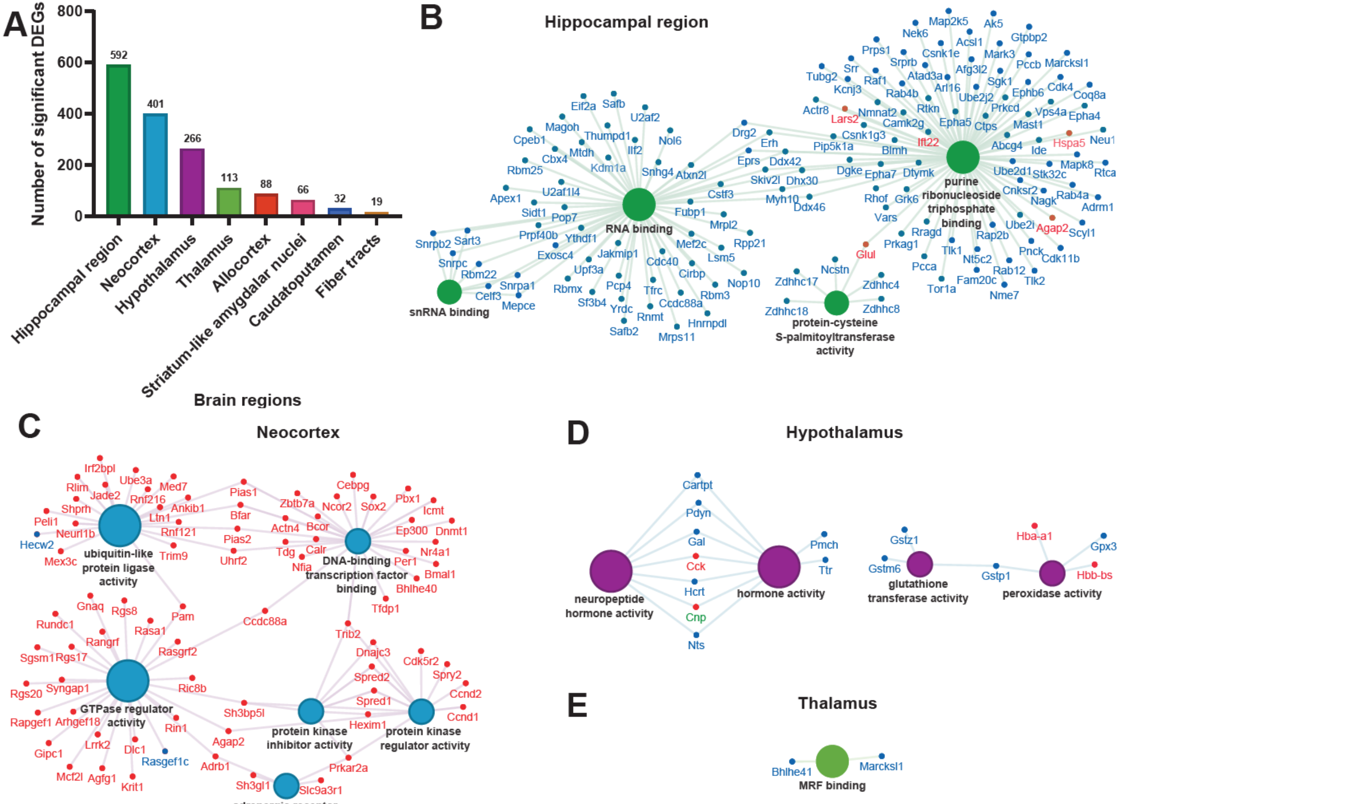

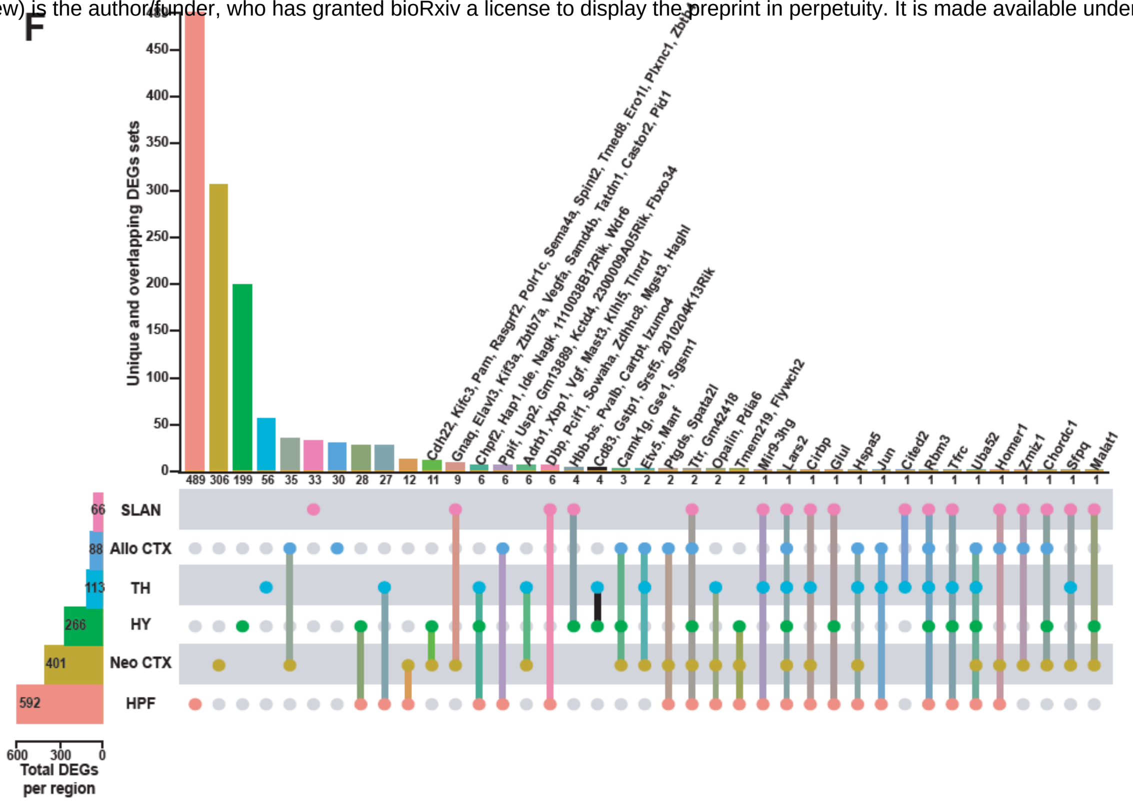

Figure 2. The hippocampal region is the brain region the most transcriptionally affected after sleep deprivation. **A**. Histogram representing the number of significant differentially expressed genes (DEGs) across each brain region previously identified. **B-E**. Molecular functions enriched from the significant DEGs in the hippocampal region (**B**), neocortex (**C**), hypothalamus (**D**), thalamus (**E**). A gene is significant if its FDR step-up < 0.001 and its log2fold-change ≥ |0.2|. The size of the circle for each enriched molecular function is proportional to the significance. Only molecular functions with a corrected p-value < 0.05 are displayed (two-sided hypergeometric test, Bonferroni step down). The DEGs within these molecular functions are color coded to show whether they are downregulated (blue) or upregulated (red). **F**. UpSet plot of interactions between each brain region that have more than 50 significant DEGs (fiber tracts and caudatoputamen excluded). The number of DEGs submitted for each brain region is represented by the histogram on the left (0-600 range). Dots alone indicate no overlap with any other lists. Dots with connecting lines indicate one or more overlap of DEGs between brain regions. The number of DEGs in a specific list that overlap is represented by the histogram on the top. For spatial expression patterns with smaller numbers of DEGs, we were able to list the gene names above their respective histogram. Genes are labeled for the smallest lists. HPF = Hippocampal Formation ; Neo CTX = Neocortex ; HY = Hypothalamus ; TH = Thalamus ; Allo CTX = Allocortex ; SLAN = Striatum-like amygdalar nuclei.

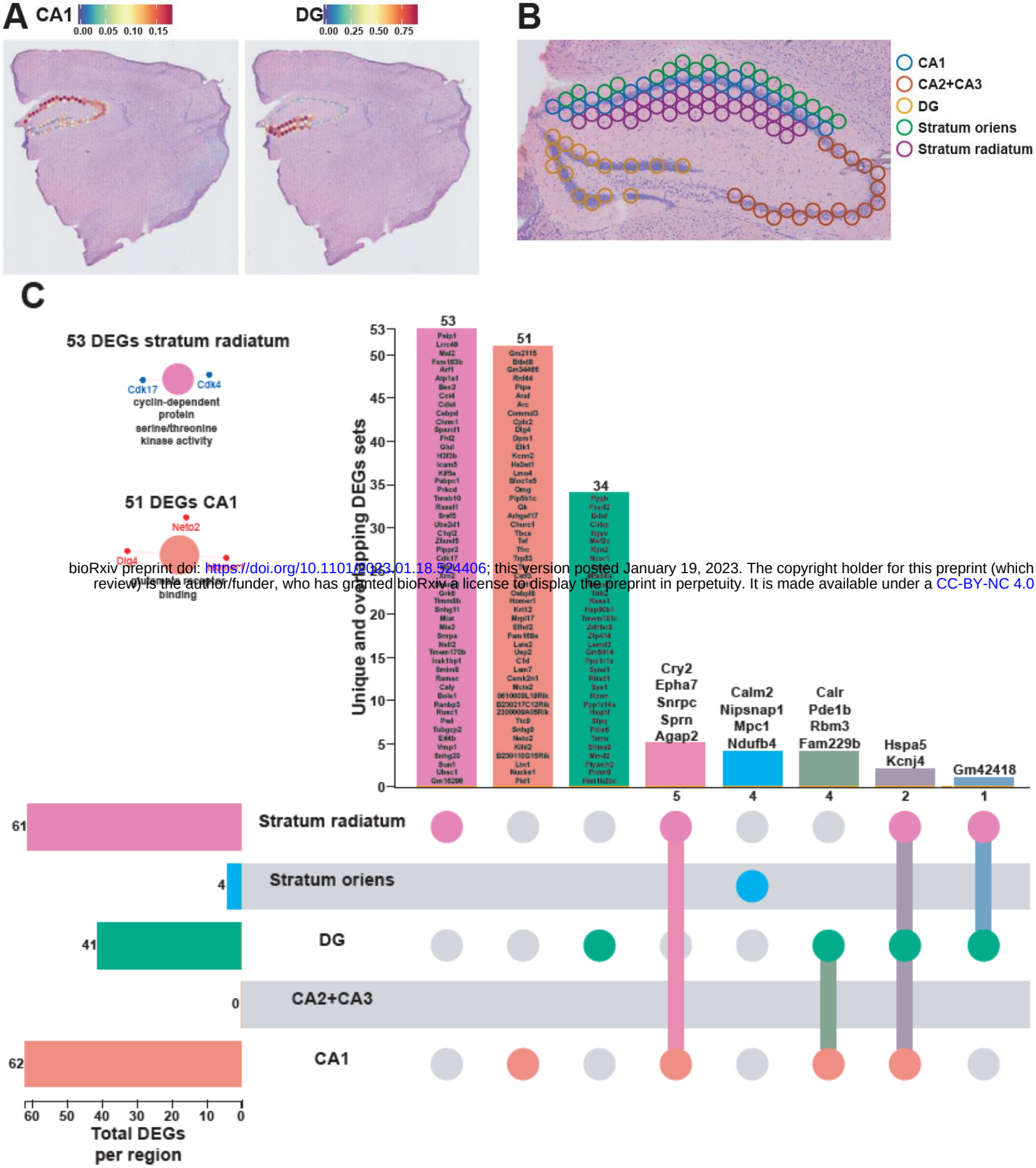

Figure 3. Each hippocampal subregions displays a unique transcriptional impact of sleep deprivation. **A**. Prediction score of the deconvolution step for each of the 2085 spots of a representative example slice for CA1 pyramidal layer and dentate gyrus granule cells are represented with the color legend from blue to red. The rest of the subregions were selected based on biological knowledge using anatomical structures apparent on the H&E staining images. **B**. Example of identified hippocampal subregions on the sample. **C**. UpSet plot of interactions between each hippocampal subregion. The number of DEGs submitted for each subregion is represented by the histogram on the left (0-62 range). A gene is significant if its FDR step-up < 0.1 and its log2fold-change ≥ |0.2|. Dots alone indicate no overlap with any other lists. Dots with connecting lines indicate one or more overlap of DEGs between hippocampal subregion. The number of DEGs in a specific list of overlap is represented by the histogram on the top. Genes are labeled for the smallest lists. The unique lists of 53 DEGs and 51 DEGs for stratum radiatum and CA1 pyramidal cells respectively enriched specific molecular functions displayed on the left. The size of the circle for each enriched molecular function is proportional to the significance. Only molecular functions with a corrected p-value < 0.05 are displayed (two-sided hypergeometric test, Bonferroni step down). A gene is considered significant if FDR < 0.001 and log2fold change > |0.2|.

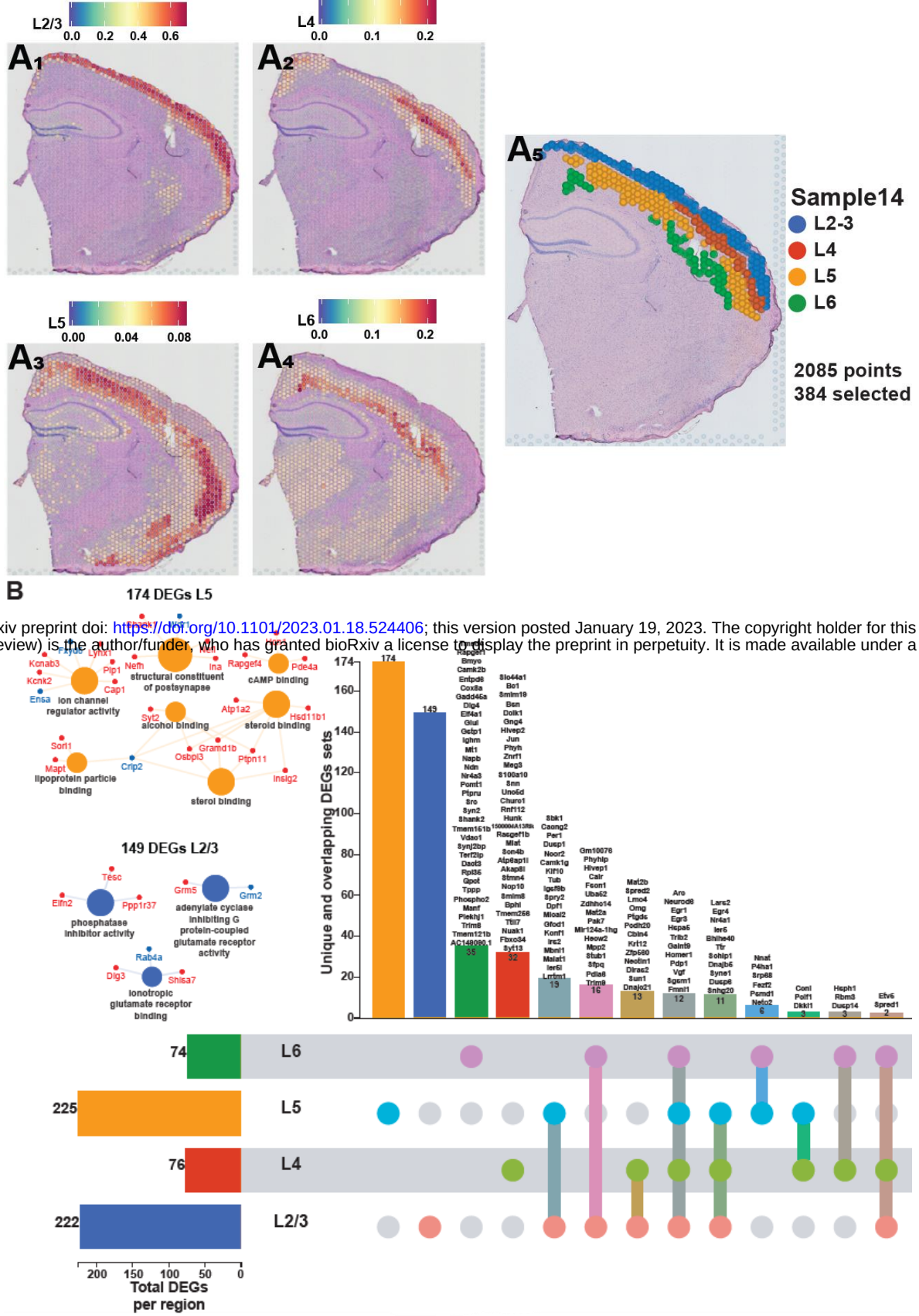

Figure 4. Each cortical layer of the neocortex displays a unique transcriptional impact of sleep deprivation. **A**. Prediction score of the deconvolution step for each of the 2085 spots of a representative example slice for each cortical layer are represented with the color legend from blue to red: layer 2-3 ($\mathbf{A_1}$), layer 4 ($\mathbf{A_2}$), layer 5 ($\mathbf{A_3}$), layer 6 ($\mathbf{A_4}$). We can distinguish between distinct sequential laminar excitatory neurons layers on the aggregated profile ($\mathbf{A_5}$). **B**. UpSet plot of interactions between each deconvoluted cortical layers of the neocortex. The number of DEGs submitted for each layer is represented by the histogram on the left (0-225 range). A gene is significant if its FDR step-up < 0.001 and its log2fold-change ≥ |0.2|. Dots alone indicate no overlap with any other lists. Dots with connecting lines indicate one or more overlap of DEGs between cortical layers. The number of DEGs in a specific list of overlap is represented by the histogram on the top. Genes are labeled for the smallest lists. L2/3 = Layer 2 and 3 ; L4 = Layer 4 ; L5 = Layer 5 ; L6 = Layer 6. The unique lists of 174 DEGs for layer 5 and 149 DEGs for layer 2/3 that enrich specific molecular functions are listed on the left. The size of the circle for each enriched molecular function is proportional to the significance. Only molecular functions with a corrected p-value < 0.05 are displayed (two-sided hypergeometric test, Bonferroni step down). A gene is considered significant if FDR < 0.001 and log2fold change > |0.2|.

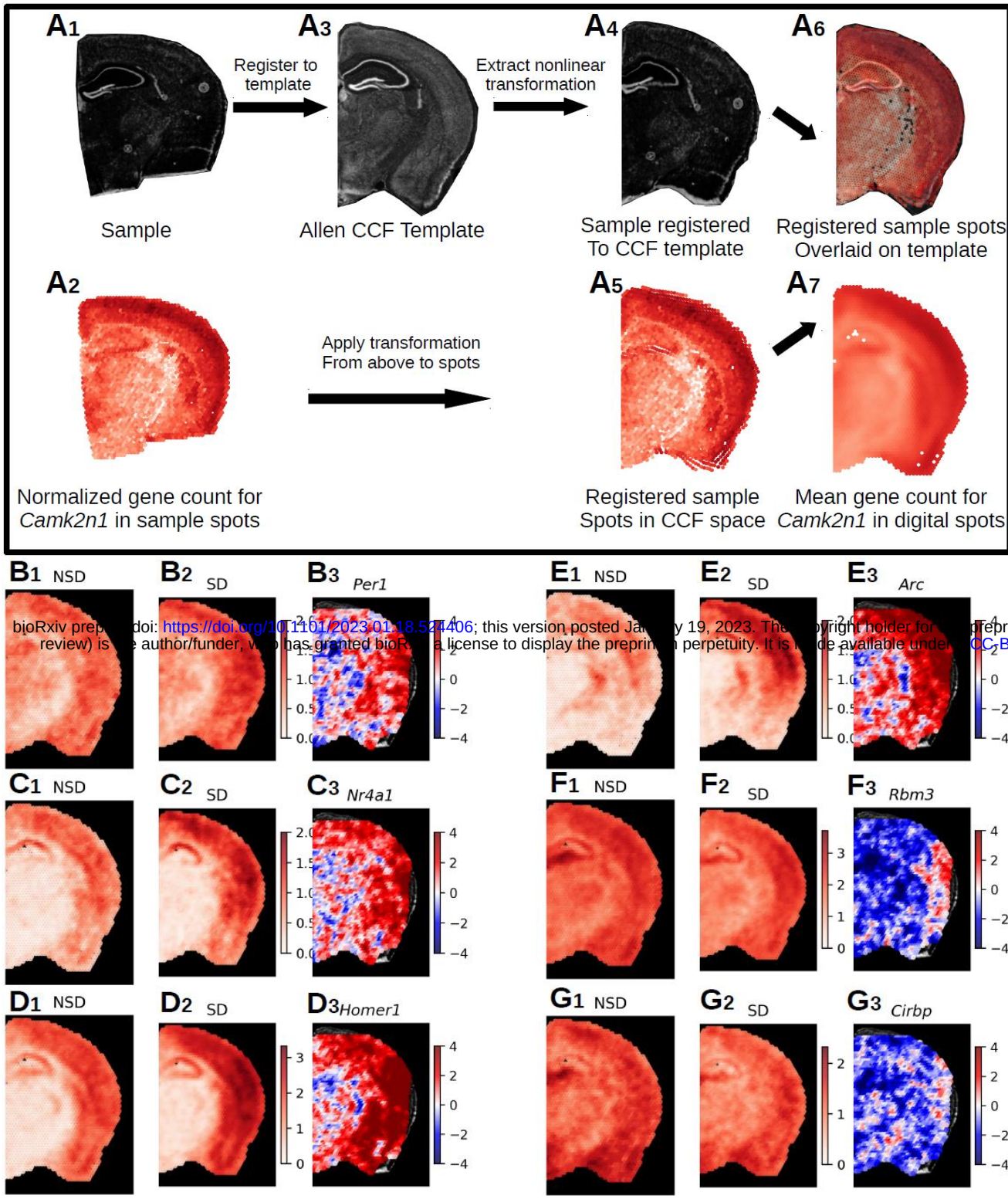

Figure 5. Registration of Visium data to Allen Common Coordinate Framework and statistical analysis of aligned transcriptomic spots. A. Nonlinear registration of the tissue image from a single Visium sample (**A_1**) and its transcriptomic spot coordinates (**A_2**) – shown as example: the gene *Camk2n1* – to the template image (**A_3**), slice 70 from the Allen P56 Mouse Common Coordinate Framework (CCF. Due to the nonlinear nature of the registration, we were able to precisely align the sample image (**A_4**) to landmarks in the template image and apply that transformation to the spot coordinates (**A_5**). To account for different numbers of spots in individual samples, digital spots spaced at 150µm in a honeycomb were created for the template slioce. Each digital spot is populated with the log base 2 normalized transcriptomic counts from the 7 nearest spots from each sample in a group (**A_7**). This approach allows the comparison of gene expression across entire brain slices in an unrestricted inference space. **B-G.** Samples were split into non-sleep deprived (NSD, n=6, 42 sample spots per digital spot) and sleep deprived (SD, n=7, 49 sample spots per digital spot). The range of the color bar for the mean calculations is set from 0 to the maximum normalized gene count for that gene for all samples, while the t-statistic color bar is bounded to [-4,4], which is approximately the equivalent to the Šidák corrected p-value of < 2.50e-05. We show a selected group of 6 genes from the 428 DEGs (Sup. Table X) (**B-G**). Panel 1 shows for each gene (B1-G1) the mean normalized gene count in NSD, panel 2 depicts the mean normalized gene count in SD (B2-G2) and panel 3 shows the t-statistics (B3-G3). The following DEGs are depicted: **B.** *Per1*, 4 significant spots. **C**. *Nr4a1*, 29 significant spots. **D**. *Homer1*, 306 significant spots. **E**. *Arc*, 168 significant spots. **F**. *Rbm3*, 31 significant spots. **G**. *Cirbp*, 9 significant spots.